Morphological, structural and optical properties of ZnO thin solid films formed by nanoleafs or micron/submicron cauliflowers

Jorge Angulo-Rocha [a], Oscar Velarde-Escobar [b], Cristo Yee-Rendón [b],
Gelacio Atondo-Rubio [b], Roberto Millan-Almaraz [c], Enrique Camarillo-García [e],
Manuel García-Hipólito [d], Francisco Ramos-Brito [a,*]

[a] *Laboratorio de Síntesis de Materiales-Facultad de Ciencias Físico-Matemáticas – Universidad Autónoma de Sinaloa, Ciudad Universitaria S/N, CP. 80000, Culiacán, Sinaloa, México*
[b] *Laboratorio de Óptica-Facultad de Ciencias Físico-Matemáticas – Universidad Autónoma de Sinaloa, Ciudad Universitaria S/N, CP. 80000, Culiacán, Sinaloa, México*
[c] *Facultad de Ciencias Físico-Matemáticas – Universidad Autónoma de Sinaloa, Ciudad Universitaria S/N, CP. 80000, Culiacán, Sinaloa, México*
[d] *Departamento de Materiales Metálicos y Cerámicos, Instituto de Investigaciones en Materiales, Universidad Nacional Autónoma de México, AP 70-360, Coyoacán 04510, DF, México*
[e] *Instituto de Física, Universidad Nacional Autónoma de México, AP 20-364, Álvaro Obregón 01000, DF, México*

ARTICLE INFO

ABSTRACT

Thin films of ZnO formed by nano and microstructures with hexagonal crystal phase were successfully synthesized by using pyrolysis technique. At first glance the films resulted divided in 7 zones that were morphologically analyzed and showed the presence of three types of particles: nano-leafs, single microparticles, and particles formed by the addition of microparticles, "clusters". The largest and therefore the main zone was formed by nanoleafs. Studies on morphology, structure and optical properties of these nanoleafs were obtained and correlated too. The knowledge acquired from these studies allowed the synthesis of nanostructured films entirely formed by nanoleafs with a width of 25 nm and a length 200 nm long regardless of the roughness of the substrate. Energy gap of 3.26 eV was invariant to changes in synthesis parameters. The studies on optical properties of nanoleafs and micro-cauliflower give an energy diagram that account for the location of the energy states introduced by native crystalline defects into the energy band gap and their radiative electronic transitions.

1. Introduction

Semiconductors in a nanometer size have been widely investigated in the past few years, there has been particular interest in correlating their optical properties with the size and shape of the nano-structures [1,2]. Recently, Zheng et al. reported the synthesis of ZnO nanocrystals with controlled size, aspect ratio, and oxygen defects via solvothermal and thermal treatment methods [3]. Their works show that the photocatalytic activity of ZnO nanocrystals is mainly dependent on the type and concentration of the oxygen defects. By other hand, obtaining ZnO as thin film significantly reduces the active surface area which is critical for the catalytic process. In order to counteract this disadvantage, many efforts have been made to produce films with convenient nanostructures that enhance the photocatalytic activity. The control of size, shape and the orientation of ZnO nano-microstructures, in particular the ability to order them into three dimensional arrays onto various types of substrates, as well as to clarify the origin of the visible emission of ZnO represent essential tasks to create functional ZnO.

Zinc oxide has always been considered one of the most important semiconductors due to its physical and/or chemical properties and the consequent multiple applications it has, which include: antireflection coatings, transparent conducting films (as electrodes in solar cells), gas sensors, varistors, surface acoustics wave devices, and electro- and photo-luminescent devices. Recently ZnO nanostructures have attracted much attention due to their potential applications in field emission displays [4,5] highly efficient optoelectronic devices [6–10], UV laser technology at room temperature [6,11] phosphors [12–14], photo-catalysis [15], electromechanical coupled sensors and transducers [16,17], spintronics [18,19], super-hydrophobicity and super-hydrophilicity sufaces [20,21], cosmetics [22], etc.

* Corresponding author.
    E-mail addresses: framosbrito@uas.edu.mx,
ramosbritof@gmail.com (F. Ramos-Brito).

Science has much further to do in the functional ZnO nanostructures direction, that is why detailed investigations of prepare methods, growth mechanisms and properties of ZnO nanostructures are needed. In the last decade, different ZnO nanostructures have been obtained by several synthesis methods [2–11,13,14,16–22]. In particular, shapes like: nanocombs, nanorings, nanohelixes/nanosprings, nanobows, nanobelts, nanowires, and nanocages have been obtained under specific conditions using only the solid-vapor phase thermal sublimation (VPTS) technique [23], which should be considered as an achievement and a proof of the well understanding of the VPTS technique by the research group involved in this investigation [23], following this idea and continuing in this direction we considered the use of spray pyrolysis (SP) technique for the synthesis of ZnO nanostructures, this considering that under certain parameter condition SP technique could involve a VPTS micro-process in every single droplet.

Using SP technique Oliviera Milosevic et al. [24], Sang Duck Lee et. al. [25] and Nora S. Portillo-Vélez and Monserrat Bizarro [26] obtain nanoparticles of ZnO. Oliviera et. al. employ ultrasonic SP with furnace tube as reactor and zinc nitrate hexahydrate as precursor. They discuss the influence of the solution concentration, the synthesis temperature and the residence time of droplets on the particle morphology. They show submicrometric as well as nanosize (100–200 nm) ZnO spherical shaped particles supported on aluminum substrate that were exposed to temperatures of: 72, 230, 588 and 892 °C and solution concentrations of: 0.004 and 1.5 mol dm^{-3}. Both studies, reported by Sang Duck Lee et. al. and Nora S. Portillo-Vélez and Monserrat Bizarro, were oriented to the photocatalytic property of ZnO nanoparticles because it confers promising application into environmental remediation, comparable to TiO_2 [27]. Sang Duck and co-workers obtain a powder composed of nanoparticles with two-types shape (spherical and crushed sphere) through an ultrasonic spray pyrolysis system with furnace tube as reactor. They employ a synthesis temperature of 900 °C and solution concentrations of: = 0.01, 0.1 and 1.0 mol dm^{-3}. Nora S. Portillo-Vélez and Monserrat Bizarro obtain two-type of films, one formed by nanoflakes and other formed by nanorods, through pneumatic spray pyrolysis with a tin bath as reactor, synthesis temperature of 450 °C, zinc acetate and zinc chloride as precursors, desionized-water and desionized-water/methanol ratio mixtures of: 100/0, 75/25, 50/50, 25/75 and 0/100 as solvents and solution concentrations of: 0.05, 0.1 and 0.2 mol dm^{-3}. Both studies, reported by Sang Duck Lee et. al. and Nora S. Portillo-Vélez and Monserrat Bizarro, show ZnO with high photocatalytic performance, but only the second one has the ZnO anchored onto a substrate, which is desirable for water treatment applications.

In this work, ZnO micro and nanoarrrays as a function of solution concentration (molarity) and synthesis temperature were synthesized by using SP technique. Low synthesis temperature values (300–450) °C without any additional treatments were employed. This in order to have nanostructured ZnO films with high active surface area and appropriated optical properties for potential applications in photocatalysis. Properties on crystalline structure, microstructure, low and room temperature photoluminescence (PL), cathodo-luminescence (CL), diffuse reflectance (DR) and Transmittance, were investigated.

2. Experimental procedure

Zinc oxide nano-/microstructures were synthesized using SP technique, which is a low cost and relatively easy scalable technique compared with other techniques that employ vacuum systems. The Fig. 1 shows the configuration of the system and the way the substrate was placed into the tubular furnace. The substrate was placed so that both sides were covered by the synthesized zinc oxide. Several samples were prepared as a function of solution concentration (M_s) and reactor temperature (T_r). The M_s values were in ranges of (0.002–0.064) mol dm^{-3}. T_r was varied from 300 to 450 °C, in 50 °C steps. The samples were labeled as Al-M_s-T_r or Si-M_s-T_r, for ZnO synthesized on aluminum or silicon substrate, respectively. The deposition time was of 5 hours and 30 min for all the samples. Precursor solution was composed of zinc acetate dihydrate [$Zn(CH_3COO)_2 \cdot 2H_2O$] in de-ionized water (resistivity = 18 MΩ). This solution was nebulized using an ultrasonic generator working at 800 kHz and then carried to the substrate by using compressed and filtered air in a flux rate of 8 Liters / min as a carrier gas. The flow rate value in precursor solution was 0.5 ml/min. The substrates were square pieces of silicon and aluminum with 1.5 cm × 1.5 cm dimensions. The aluminum and silicon substrates were obtained from commercial aluminum and silicon wafer with (100) preferred orientation, respectively. The aluminum substrates were sanded previous to zinc oxide deposition in order to clean and scratch theirs surfaces. One of the two surfaces of the silicon substrate came etched from factory; this surface shows a square tessellate.

In order to investigate about the origin of the visible emission, the Si-032-450-O25-N75 sample was synthesized changing the carrier gas of filtered air with a mixture of 75 % nitrogen and 25 % oxygen; using silicon as substrate, Ms = 0.032 mol dm^{-3} and Tr = 450 °C. Nitrogen and oxygen gases were from Praxair Co. Once the film was analyzed by PL spectroscopy, it was subjected to the following high temperature heat treatment: room temperature (T_{room}) – 500 °C in 6 h, remains at 500 °C for 1 h, 500–700 °C in
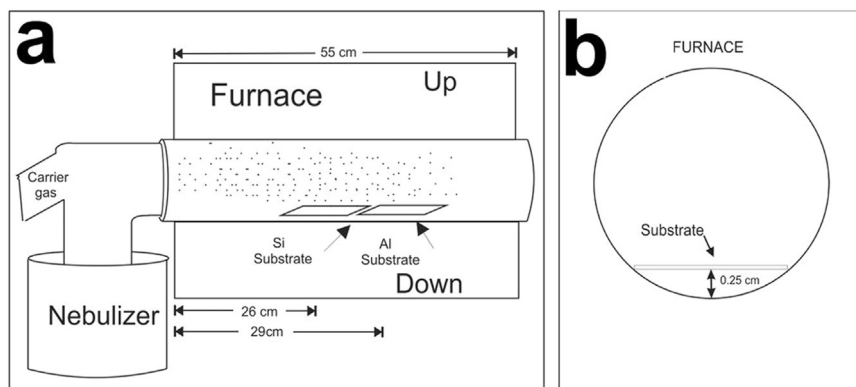

Fig. 1. a) Configuration of the system employed for the synthesis of the ZnO films. b) Diagram of the transversal section that indicate how the substrates were placed into the tubular furnace.

3 h, remains at 700 °C for 1 h, then it is allowed to reach T_{room} inside the oven. And then was analized by PL spectroscopy again.

Micrographs to explore the morphology of the samples were obtained with a Leica Cambridge Stereoscan 440 Scanning Electron Microscope (SEM). Crystalline structure was analyzed by x-ray diffraction (XRD), using a Broker-axs D8-advance with Cu Kα radiation at 1.5426 Å. Identification of hexagonal phase and indexing of the peaks for XRD patterns were carried out by using XRD-PDF cards provided by ICCD with associated numbers: 00-036-1451 for zinc oxide, 00-004-0831 for zinc and 00-004-0787 for aluminum. The grain size (t) was calculated by using Scherrer formula [28].

The 355 nm emission line of a 10 ns Nd:YAG pulsed laser model Quanta-Ray of Spectra Physics was employed as excitation source to obtain T_{room} and 18 K PL spectra of the samples. A filter was used to reject the 532 and 1064 nm laser lines. The emission spectra were recorded using a conventional setup. The sample was placed in a mobile holder for aligning purpose, which was inside a compressed-helium cryostat of Air Products. The emission was collected perpendicular to the pumping signal. A monochromator, model SpectroPro 2500i of Acton Research Corporation, was used to scan the emission spectrum and then measured using a photomultiplier tube, model R-930 of Hamamatsu, connected to a PC through a Lock-in amplifier, model SR530 of Stanford Research Systems. Both slits of the monochromator were placed at 100 μm.

The excitation and emission PL spectra at T_{room} of sample Si-032-450-O25-N75 were obtained using a spectrofluorimeter FluoroMax-P brand, Jobin Yvon Horiba with a resolution < 2 nm, the lamp intensity correction is performed automatically by this instrument, which measures the excitation light intensity with an additional photomultiplier tube and performs the correction accordingly before displaying the data. Diffuse reflectance and Transmittance measurements in a range of (200–900) nm were carried out by employing a VARIAN Cary 5000 UV–vis-NIR Spectrophotometer and considering the polytetrafluoroethylene as reference material for DR = 1. CL spectra were achieved in a stainless steel vacuum chamber with a cold cathode electron gun (Luminoscope, model ELM-2; MCA, Relion Co.) Samples were placed inside the vacuum and evacuated to 10^{-3} Torr. The electron gun was deflected at 90 °C to bombard the luminescent material perpendicular to the surface. The accelerating voltage and the applied current were varied in a range of (1–15) kV and (100–600) μA. The spot size of the electron beam on the sample surface was approximately 5 mm in diameter, which implies current densities in a range of (0.5–3.1) mA/cm^2. The light emitted from the sample was collected by an optical fiber and fed into the spectro-fluorimeter FluoroMax-P brand, Jobin Yvon Horiba to be analyzed. All CL spectra were obtained at T_{room}.

3. Results and discussion

3.1. Morphology

All samples deposited on aluminum or silicon show both substrate sides covered by synthesized ZnO. At first sight it is evident that the deposition on the top side, for all samples, was not uniform along the substrate surface, while the underside looks uniform. The top side of the substrate presents a deposition pattern like it Fig. 2i. This pattern is associated to the differences in quantity of ZnO deposited on the zones as
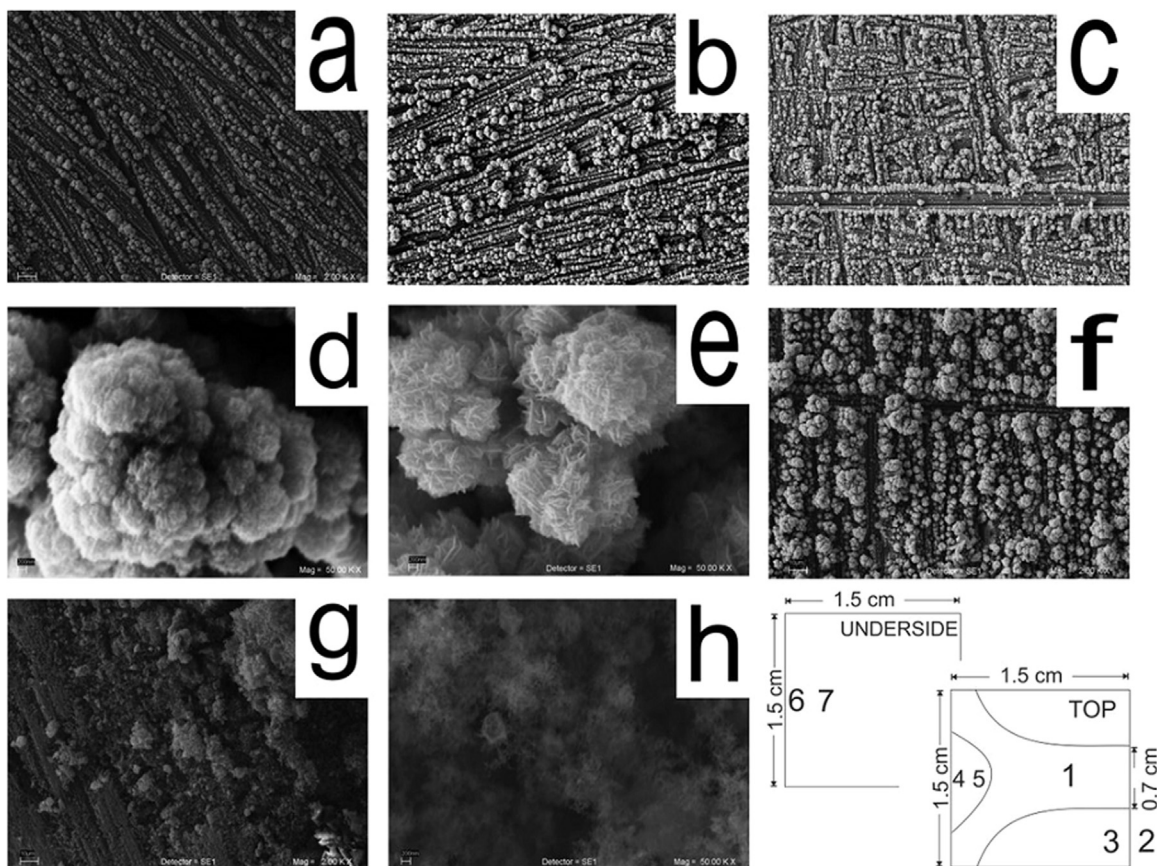

Fig. 2. Micrographs from the different zones of the Al-064-450 sample. a) Zone 1, b) Zone 5, c) Zone 7 d) Zone 4, e) Zone 6, f) representative micrograph of zones 4 and 6 g) Zone 2, h) Zone 3, i) Deposition pattern of the films over the substrate, top & underside.

product of aerodynamics of gaseous reactants. Even when at first glance a homogenous deposition was observed in the underside of all samples, two different zones were selected for analysis, zone 6 and 7.

Fig. 2 shows micrographs of the seven zones of Al-064-450 sample which is representative of all samples deposited on aluminum at same molarity and different temperature. After an inspection by SEM of every zone of the samples, all of them practically present the same morphology except the zones 2 and 3 where zinc oxide has fiber appearance with certain porosity (see Fig. 2g, h). Zinc oxide films synthesized by a similar technique showed a same behavior presenting different morphologies. [24–26,29].

The scratched surface of aluminum substrate was observed in the seven zones. The surface of the sample in the central zones of the substrate, 1, 4, 5, 6 and 7, show the presence of three types of particles: nano-leafs, single microparticles, and particles formed by the addition of microparticles, "clusters". All microparticles have the same cauliflower shape constituted by nanoleafs. The microparticles have preference to grow in the edges of the scratches probably due to the major concentration of surface defects that act as nucleation centers in addition with the possible localized turbulent aerodynamic processes which improve the synthesis process. At first glance, the relative quantity of microparticles as a function of size and their distribution along zones 1, 5 and 7 look almost the same (Fig. 2a,b,c), indicating similar roughness between those zones. All microparticles in zones 1, 5 and 7 have size less than five microns predominating three sizes: one, three and five microns; while zones 4 and 6 show a great number of microparticles with size notably bigger than five microns, even there are several particles of size around twenty microns (Fig. 2f). This confers major roughness and thickness in zones 4 and 6 which is associated with bigger deposition rate in these zones [30].

The micrographs of cauliflowers in zones 4 and 6, Fig. 2d and e, respectively, show that cauliflowers synthesized on top of and the underside of the substrate are slightly different. Both are formed by nanoleafs but the cauliflowers in zone 6 exhibit a more rugged surface as a consequence of bigger nanoleafs.

Fig. 3a and b show micrographs from two different points of zone 1 in Al-032-450 sample. In these micrographs that are representative of zone 1, it is notable how the nanoleafs cover all surface reaching to texturize it, even more, they seem vertically oriented (Fig. 3c). The absence of cauliflowers can also be observed, even when several micrographs from different points in zone 1 were obtained. This suggest that at lower Ms values the surface can be covered only by nanoleafs regardless of the roughness of the substrate. The nanoleafs have a width of 30 nm and a length 200 nm long.

Fig. 4 shows micrographs of ZnO synthesized on both surfaces of silicon substrate, where its polished and etched surfaces were considered its top and underside, respectively. After an inspection by SEM of the seven zones of Si-016-450, Si-032-450 and Si-064-450 samples, two facts were notable: a) zones 1, 4 and 5 present practically the same morphology which is represented by Fig. 4e and f, and b) the zones 6 and 7 exhibit the same morphology, analogous to zone 6 in Al-064-450 (Figs. 4a, b, c and 2f). In zones 1, 4, and 5, the Si-Ms-450 films show a flat surface which is homogeneously formed by nanoleafs and without presence of cauliflowers. In particular, for Si-032-450 film, the nanoleafs have a width of 30 nm and a length 200 nm long (Fig. 4e), similar to the nanoleafs in the Al-032-450 sample.

Fig. 4a, b and c show micrographs from zone 6 in Si-016-450, Si-032-450 and Si-064-450 films, respectively. At first glance, the samples show a surface covered by cauliflower particles of micron and submicron dimensions (Fig. 4a, b and c). The increase in quantity and size of the particles is quite noticeable as M_s
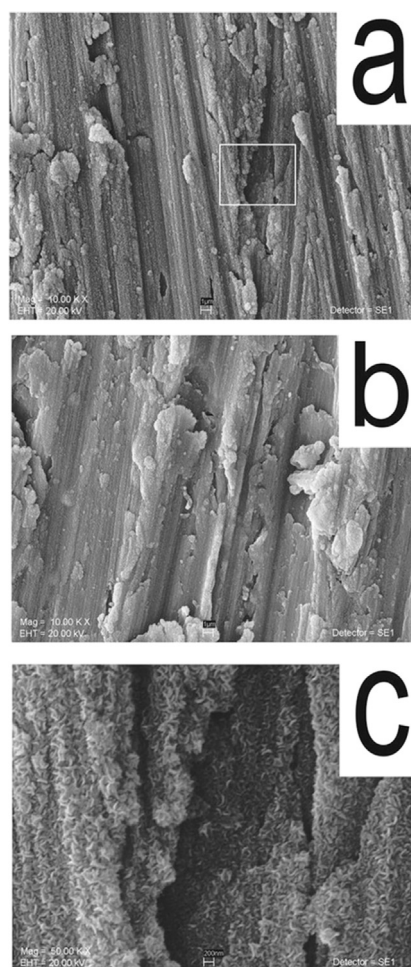

Fig. 3. Micrographs from two different points located in zone 1 of the Al-032-450 sample (a) and (b). Zoom of point 1 (c).

increases, which makes it possible to cover the holes along the entire etched surface. In sample Si-016-450 (Fig. 4d) that was synthesized by employing lower Ms value, there are three kind of particles covering the etched surface: cauliflower shaped particles with micron (3) and submicron (2) dimensions, and nanoleafs (1). In the bottom of the hole, single nanoleafs are present and the superposition of them to form cauliflowers becomes evident when you pass the view from the inside out of the hole. This allows observing the different stages in the growth of cauliflowers which are labeled in the micrograph: 1) nano-leaf; 2) cluster of nano-leaf to form submicron cauliflowers; 3) clusters of submicron cauliflowers to form micro cauliflowers. There is no preference in the orientation of nano-leafs when they superimpose to form cauliflowers. These cauliflowers have preference to grow in the edges of the upper part of the holes, analogous to the cauliflowers in the edges of the scratches in Al-064-450 (Fig. 2f). In Si-032-450 and Si-064-450 films, Fig. 4b and c, only particles with cauliflower shape are present and they are very similar to the particles deposited in zone 4 or 6 of the Al-064-450 film (Fig. 2f).

3.2. Crystalline structure

The measurement of XRD patterns of the samples consider the top side of the sample and therefore the zones that comprise it. Fig. 5a and b shows the XRD patterns for samples Al-Ms-450 and Al-0.032-Tr as a function of: Ms and Tr, respectively. Both kind of results show three peaks with mayor intensity centered at $2\Theta =$ 37, 45 and 65° that correspond to aluminum substrate, the other
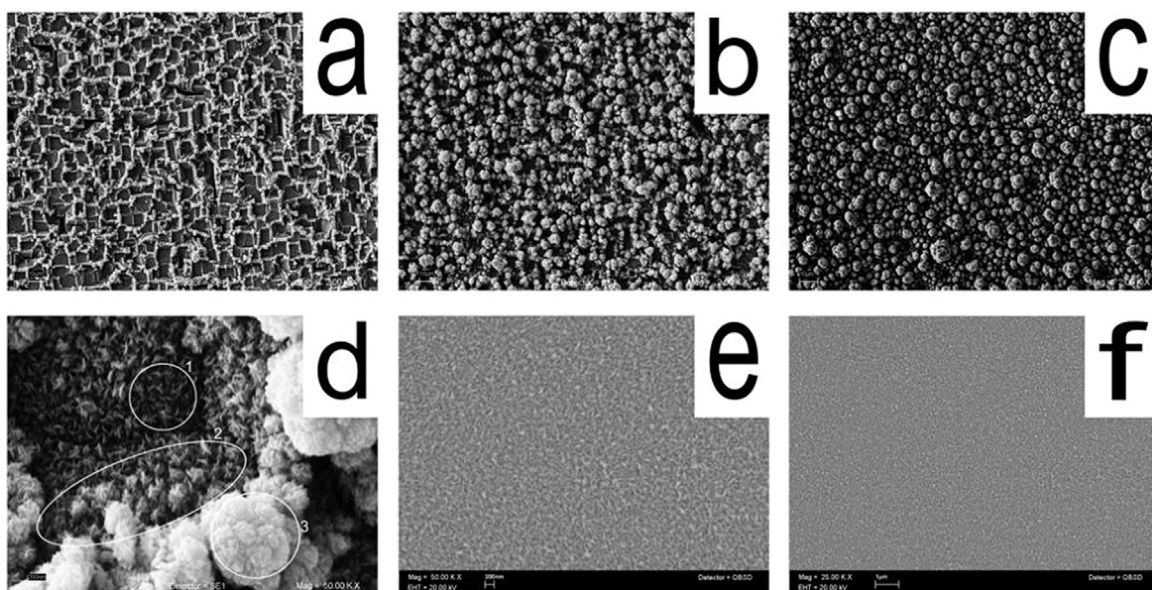
Fig. 4. Micrographs of ZnO synthesized on both surfaces of silicon substrate. a) Zone 6 of Si-016-450 sample, b) Zone 6 of Si-032-450 sample, c) Zone 6 of Si-064-450 sample, d) Zoom of the zone 6 of Si-016-450 sample, e) Zoom of the zone 5 of Si-032-450 sample and f) Zone 5 of Si-032-450 sample.
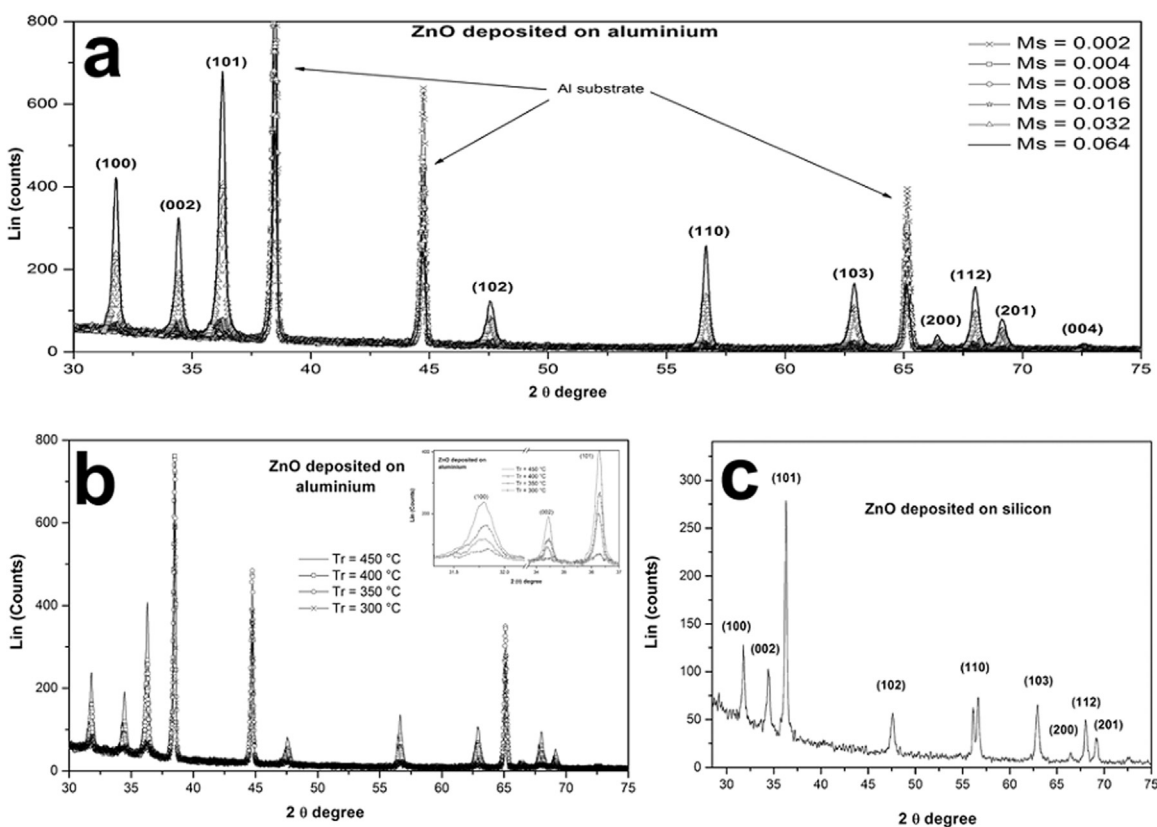

Fig. 5. XRD pattern for the sample labeled as: a) Al-Ms-450 as a function of Ms, b) Al-0.032-Tr as a function of Tr. The inset shows broadening of the spectrum corresponding to the peak area (100), (002) and (101) and c) Si-032-450.

peaks were associated with planes of the hexagonal crystal phase of ZnO. The absence of diffraction peaks or apparition of new ones did not happen when Ms or Tr varied, even neither shifts in 2Θ values for the centres of all peaks were not observed, indicating no change in the crystalline phase and nor deformation of the crystal lattice of cauliflowers and nanoleafs. This is in agreement with the fact that cauliflowers were formed by nanoleafs. The lattice para-meters were: a = 3.25 and b = 5.20 A. It is notable that the

intensity of ZnO peaks increases while aluminum-substrate peaks decrease, when both Ms and Tr increased, indicating an increase in deposition rate that gives rise to films with higher thickness, in agreement with SEM micrographs 2a and 3b.

The values for: I(100) / [I(100) + I(002) + I(101)] , I(002) / [I (100) + I(002) + I(101)] and I(101) / [I(100) + I(002) + I(101)] ratios as a function of Ms and Tr were calculated, to determine the variation of the relative intensity between the peaks (100), (002)
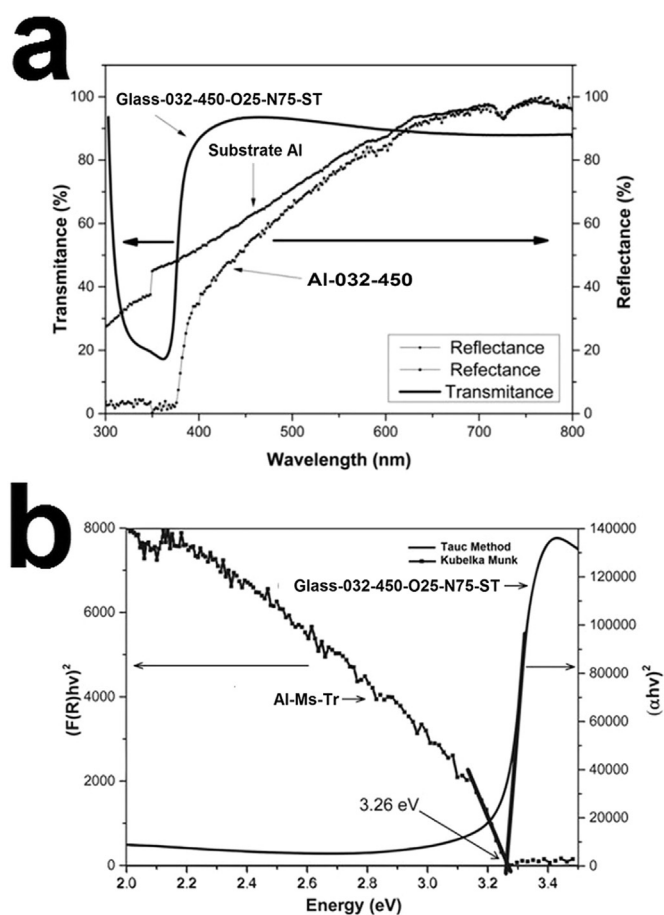
Fig. 6. a) Representative DR spectrum of Al-Ms-Tr samples as well as the DR spectrum of Al substrate. Transmittance spectrum of Glass-032-450-O25-N75-ST b) Kubelka Munk´s curve of Al-Ms-Tr samples. Tauc´s curve of Glass-032-450-O25-N75-ST.

and (101). The peak (100) shows an increment of 16.5 % when Ms increases, while the peak (002) shows an increment of 20.8 % when Tr increases, indicating a moderate preferred growth of ZnO in those directions when Ms and Tr increase, respectively.

The values for grain size as a function of Ms were: 27, 35 and 34 nm for Ms = 0.016, 0.032 and 0.064 mol, respectively, there is an increase in grain size when Ms increases until reaching an optimal value of around 35 nm for Ms = 0.032 mol and remains constant, while grain size do not depends on Tr and remains constant in 35 nm for Tr values > 350 °C.

Fig. 5 shows the XRD pattern of Si-032-450 sample, whose peaks match very well with XRD peaks of ZnO films grown over aluminum, indicating no changes in crystalline structure as substrate changes. The grain size was of 34 nm, similar to samples deposited over aluminum, which was calculated from peaks (100), (002) and (101).

3.3. Optical properties

Optical measurements were done over Al-032-450, Si-032-450 and Al-064-450 samples, only over zone 1, where nanoleafs and/or cauliflower were deposited (see Figs. 2a and 3), no other zone was considered.

Fig. 6 shows the representative DR spectrum of Al-032-Tr samples and its Kubelka Munk curve [31], as well as the DR spectrum of Al substrate. The substrate shows a decrement in reflectance starting from 650 nm that increases as the wavelength decreases. This behavior was associated with the surface

roughness and its consequent light scattering on it. The DR spectra for ZnO films show the same behavior due to the fact that ZnO deposition tends to preserve the roughness of the aluminum substrate, this was shown above in the morphology section (Fig. 3c). Besides light scattering, ZnO nanoleafs show a relatively narrow "near band edge" zone that was mostly associated to surface crystalline defects. The band gap obtained from Kubelka Munk curve analysis was of 3.26 eV (Fig. 6b).

ZnO is a direct band-gap semiconductor with wide band-gap energy ($\sim$3.37 eV) at room temperature and a very large exciton binding energy of about 59 meV which allows for more efficient excitonic emission at room and higher temperatures [32–34]. Commonly, photoluminescent studies on ZnO nanostructures report a strong near-band-edge UV photo-luminescent peak in a range of (370-390) nm [35–38], which corresponds to energies in a range of (3.2–3.35) eV, resulting from an excitonic type recombination. There is a typical visible emission too in the blue-green region as a result of deep energy levels in the forbidden band gap of ZnO, coming from structural defects in the ZnO crystal lattice [35–40]. These structural defects act as traps for carriers, and have been mainly attributed to surface defect levels associated with oxygen vacancies or zinc interstitials in the ZnO crystal lattice [39–41]. Up to now, the origin of the green emission is highly controversial and with several hypotheses [42], it is attributed to surface defects, as was mentioned before, but the nature of these defects is still not fully understood [42]. However, research reported by FAN Hai-Bo et. al. [43] and G. H. Mhlongo et. al. [44] are really convincing as they show convincing results. FAN Hai-Bo et. al. study the origin of green and yellow emission by using PL and x-ray photoelectron spectroscopy (XPS) and by combining the two results it is deduced that the green luminescence (GL) and yellow luminescence (YL) are related to the V_O and O_i defects, respectively. Whereas G. H. Mhlongo et. al study the origin of violet-blue emission by using Raman, PL, XPS and electron spin resonance (ESR) and a combination of results suggest that Zn related defects; especially V_{Zn} and Zni are the primary source of violet-blue emission.

The cathodoluminescence spectra of Al-064-450 sample as a function of acceleration voltage (Av) is presented in Fig. 7. Inset of Fig. 7 shows their normalized CL spectra. It is shown that the CL spectra curve shows slight changes in shape as Av varies, thus indicating homogeneity in chemical composition, and slight changes in relative density of defects in the cauliflowers, as a function of its depth. The two emission bands centered at 390 (violet-blue) and 512 nm (Green-Yellow) of the CL spectra are in agreement with research presented by FAN Hai-Bo et. al.[43] and G. H. Mhlongo et. al [44]. Both bands are asymmetric and structured. The Gauss fitting of the CL spectrum of ZnO cauliflowers (Al-064-450) shows resolved emission peaks at: 377, 382, 390, 401, 426, 468, 508, 565, and 662 nm (Fig. 11a). The 377, 382, 401 and 426 nm emission peaks are in agreement with the Gauss fitting proposed by G. H. Mhlongo et. al [44] and were associated to: a) 377 and 382 nm (3.25–3.29 eV) emission peaks correspond to electronic transition from conduction band (CB) to valence band (VB) and excitonic recombination, b) 401 nm (3.09 eV) emission peak can be ascribed to the electron transition from the bottom of the conduction band to the V_{Zn} level and c) 426 nm (2.91 eV) emission peak corresponds to the energy interval from the donor level of Zn_i to the top of the valence band [45], in agreement with the excitation peak centered at 418 nm in the PL excitation spectrum for emission wavelength (λemiss) = 450 nm showed in Fig. 10. The 508 and 565 nm emission peaks are in agreement with the Gauss fitting proposed by FAN Hai-Bo et. al. [43] and were associated with V_O and O_i defects, respectively. The 508 nm (2.44 eV) emission peak was associated with $V_O \rightarrow V_{Zn}$ electronic transition which is supported by the excitation peak centered at
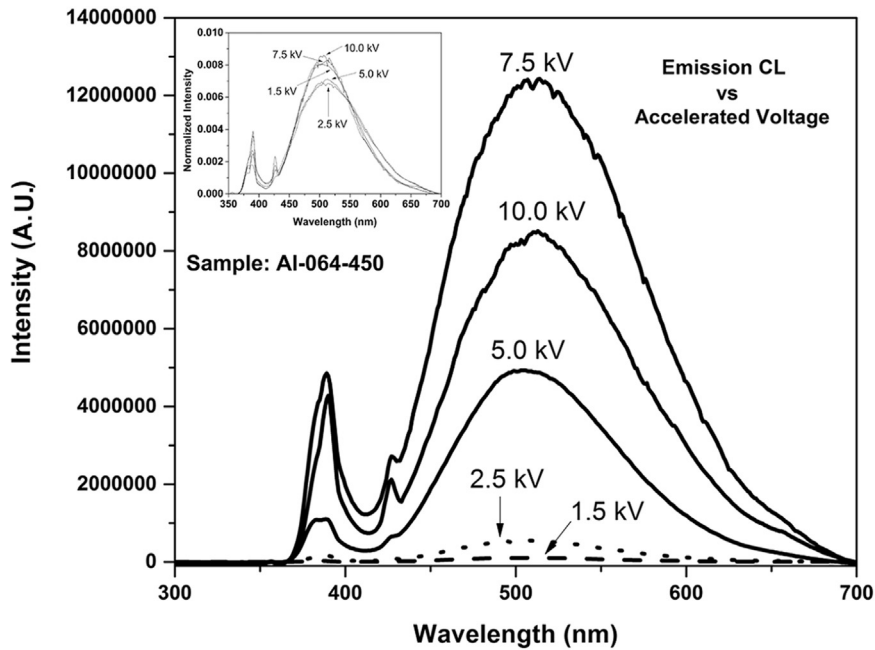
Fig. 7. Cathodoluminescence spectra of ZnO cauliflowers (Al-064-450 sample) as a function of acceleration voltage (Av). Inset shows the normalization of the CL spectra.

468 nm in the PL excitation spectrum for $\lambda_{emiss} = 500$ nm (inset of Fig. 10). The 565 nm (2.19 eV) emission peak was associated with CB $\rightarrow$ O_i electronic transition [46]. The 390 nm (3.18 eV) emission peak was ascribed to shallow donors sites at 0.08 eV below the CB, commonly associated to neutral interstitial zinc (Zn_i^0) and oxygen vacancies (V_O^0), consequently to electronic transitions: $Zn_i^0 \rightarrow VB$ and $V_O^0 \rightarrow VB$ [46]. Then, once the location of energy states introduced by Zn_i^0/V_O^0, V_{Zn}, Zn_i, V_O and O_i into the energy band gap have been established, evidently and automatically the 468 nm (2.65 eV) emission peak must be associated with $V_O \rightarrow VB$ electronic transition. This is in agreement with: results shown by Yuanhui Zheng et. al [47], the prescence of excitation peak

centered at 468 nm in the PL excitation spectrum for $\lambda_{emiss} = 500$ nm (inset of Fig. 10) and that the quenching of 466 nm emission peak occurring after annealing (Fig. 11c).

Fig. 8 shows the PL spectra of Al-032-450, Al-064-450 and Si-032-450 samples measured at T_{room} and $T = 18$ K. The normalization of the spectra shows that PL emissions from cauliflowers (Al-064-450), nanoleafs synthesized on aluminum (Al-032-450) and nanoleafs synthesized on silicon (Si-032-450) are very similar between them. The comparison shows that visible emission band does not suffer significant changes (inset of Fig. 8) while maximum in exciton emission undergoes a blue shift, going from 384 to 375 nm and its FWHM decreases (Fig. 8 and Fig. 11b). The average
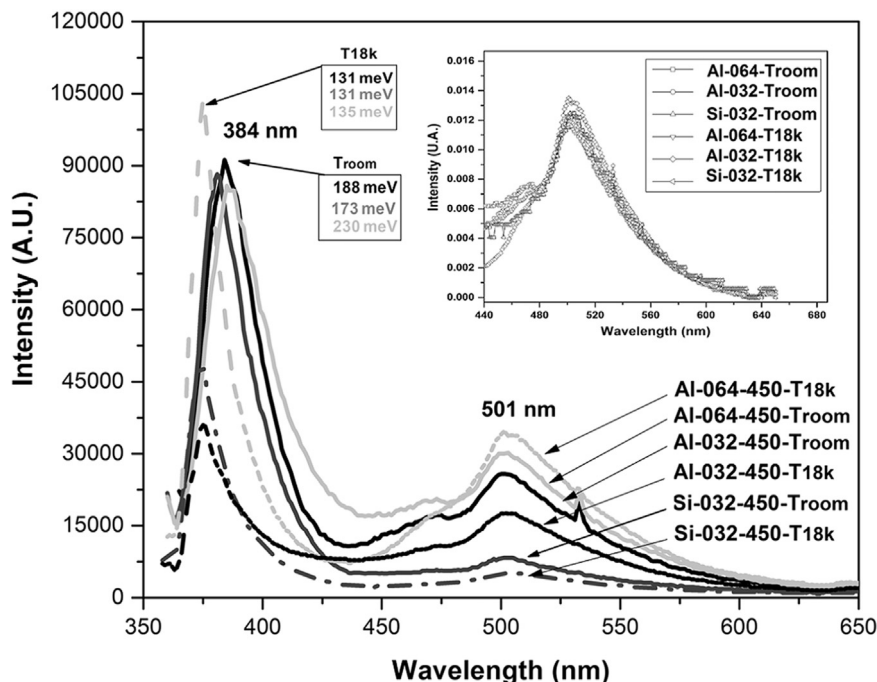

Fig. 8. a) PL spectra of the Al-032-450, Al-064-450 and Si-032-450 samples at two different temperatures: T_{room} and 18 K. Inset shows the normalized PL spectra in the visible region.
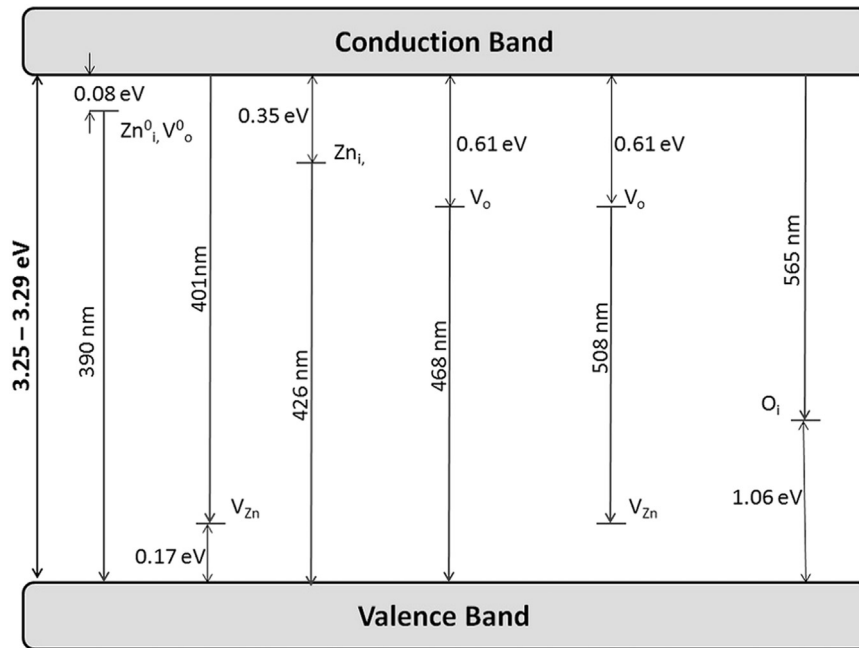
Fig. 9. Energy diagram that shows indistinctly the different de-excitation paths for nanoleafs or cauliflowers.

FWHM varies from 197 meV for T_{room} to 132 meV for T = 18 K. The cauliflowers (Al-064-450) experimented the biggest narrowing of the exciton emission band of around 95 meV when temperature goes from T_{room} to 18 K. With regard to the visible emission, only the nanoleafs synthesized on silicon (Si-032-450) shows a minor intensity (Fig. 8), but PL spectrum preserves its curve shape (inset of Fig. 8), which indicates nanoleafs with bigger optical quality and same kind of crystalline defects when they are deposited on silicon. The invariability of the shape between the PL spectra for cauliflowers (Al-064-450) or nanoleafs (Al-032-450) in addition with SEM results indicate that cauliflowers are formed by nanoleafs.

Fig. 9 integrates the analyses of CL, PL, DR and Transmittance spectra of the ZnO films in an energy diagram that shows indistinctly the different de-excitation paths for nanoleafs or cauliflowers. This energy diagram resulted in good agreement with studies reported by many research groups [41,48–53].

The PL spectra are similar to CL spectra. Fig. 11b shows the Gauss fitting of PL emission spectrum of Al-032-450 sample, which is representative of T_{room} spectra in Fig. 8. It notable that PL emission is similar to CL emission (Fig. 11a) because it practically shows the same emission peaks. Only the 426 nm emission peak of CL spectrum, associated with $Zn_i \rightarrow$ VB electronic transition, is absent in PL spectrum Fig. 11b. This indicates that excitation with
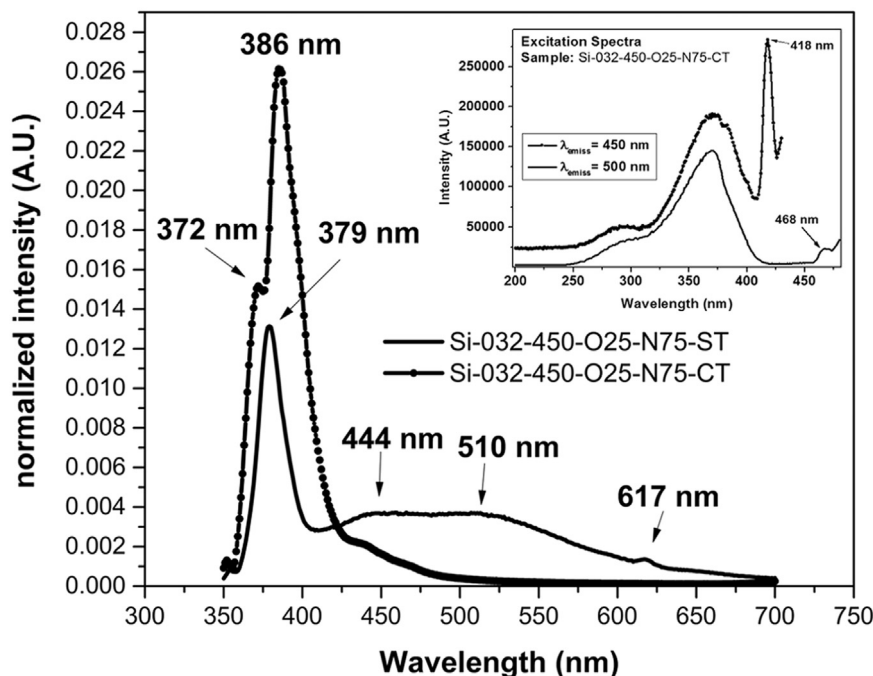

Fig. 10. PL emission spectra of Si-032-450-N75-O25 sample with thermal annealing (CT) and without thermal annealing (ST). Inset shows the PL excitation spectra of Si-032-450-N75-O25-CT for λ_{emiss} = 450 and 500 nm.
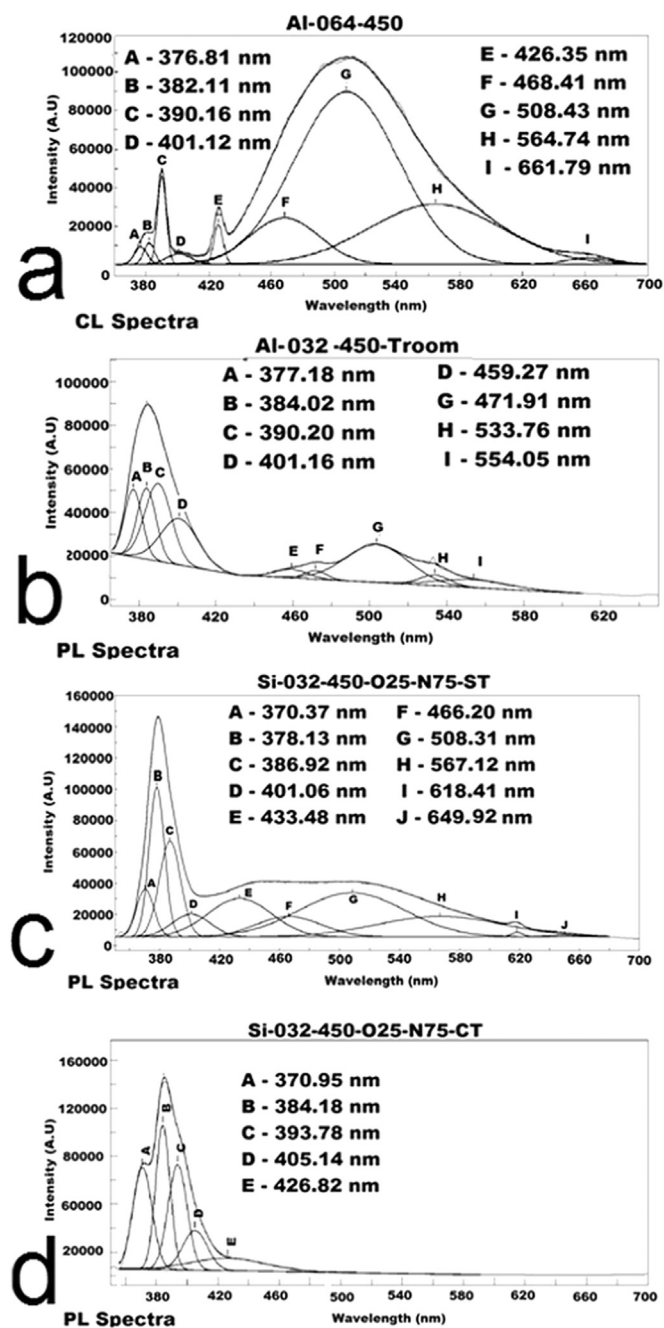
Fig. 11. Gauss fitting for: a) CL spectrum of ZnO cauliflowers, b) PL emission spectrum for nanoleafs synthesized on aluminum, c) PL emission spectrum of nanoleafs synthesized on silicon and d) PL emission spectrum of the nanoleafs that were synthesized on silicon and suffered annealing treatment.

or electron–hole pairs produced by an incident electron depends on its energy and the nature of the sample. The recombination of electron–hole pairs can produce photon emission. Therefore, as the electron-accelerating voltage increases, the penetrating electrons can produce more electron–hole pairs, due to the interaction with a larger volume of the luminescent material, to result in an increase of CL intensity. Also, the production of secondary electrons is important to the CL-generation process, since they can generate electron–hole pairs along the entire electron zigzag path during its energy dissipation, which may be many micrometers in length [55]

In order to verify that the 565, 508 and 468 nm emission peaks are related to intrinsic defects and not with unwanted impurities coming from filtered air, nanoleafs over silicon substrate were synthesized again (Si-032-450) but now using a mixture of 75% nitrogen and 25% oxygen as carrier gas instead of filtered air, the sample was renamed as Si-032-450-O25-N75-ST. The same sample was synthesized over Corning glass to obtain its transmittance spectrum and Tau´s curve showed in Fig. 6. The Fig. 10 shows PL emission spectrum of Si-032-450-O25-N75-ST. This was formed by an intense peak centered at 379 nm and a broad band over the entire visible region. This emission spectrum is very similar to PL emission spectrum of nanoleafs synthesized by using filter air as carrier gas (Si-032-450) but there is a remarkable difference, when an oxygen/nitrogen mixture carrier gas is used the emission centered at 433 nm appears with a very high relative intensity (Fig. 11c). Which results in an increase of Zn_i defects. The relative emission intensity associated to the visible region of these nanoleafs (Si-032-450-O25-N75-ST) is intense compared to the first ones nanoleafs (Si-032-450) as can be seen from their respective emission spectra in Figs. 10 and 8, respectively. The variation in the PL intensity indicated that filtered air probably increases the concentration of defects because it has unwanted impurities that can act as recombination centers for charge carriers. "If the density of defects is high enough, the defects will mainly behave as the recombination centers, thus leading to the PL intensity decrease with the increase of defect density" [44]. Once the Si-032-450-O25-N75 sample is subjected to an annealing process, its PL emission in the visible region practically disappears (Figs. 10 and 11d) which indicates a remarkable lessening of the density of defects, including Vo, O_i, V_{Zn} and Zn_i, resulting in quenching of the visible emission.

The presence of the 370 nm emission peak in PL emission spectra of Si-032-450-O25-N75 (Fig. 11c and d) was associated to the blue shift of the excitonic recombination due to quantum confinement effect. The increase of its intensity after annealing indicates the formation of nanocrystals due to recrystallization process.

3.4. Potential use of micro-cauliflowers and nanoleafs in photocatalysis.

The ZnO nanoleafs synthesized in this work shows improved properties compared to those nanoflakes synthesized by Nora S. Portillo-Velez and Monserrat Bizarro [26]. Nanoleafs show lower physical dimensions which gives to the ZnO film greater surface-to-volume ratio and consequently should have greater photocatalytic activity. Films formed by nanoleafs have higher I(100)/I(002) intensity ratio than formed by nanoflakes. Recently, Anna Mclaren et. al. reports that higher I(100)/I(002) intensity ratio in hexagonal ZnO leads to greater photocatalytic activity [56]. Then, as the ZnO cauliflowers synthesized in this work were formed by these ZnO nanoleafs so they should have improved properties compared to those nanorods synthesized by Nora. The physical dimensions of the cauliflowers can be changed by varying Ms (Fig. 4a, b and c) and with it optimize the surface – to – volume

355 nm from NdYAG laser do not promote the radiative decay through Zn_i defects, even when electrons should be excited from VB to CB, more studies are needed to elucidate this.

Unlike CL spectra, the PL spectra show a structured visible emission with several local maxima. The missing of this kind of structure in the CL emission spectra is due to its intense emission. Surely, the structure was masked by the big intensity of CL emission. In CL spectroscopy, incident electrons interact with specimen atoms and are significantly scattered by them (rather than penetrating the sample in a linear fashion). Electrons that penetrate the sample can eject bound electrons, generating secondary electrons, or excite a valence electron to the conduction band, creating electron–hole pairs [54]. The quantity of secondary electrons and/

ratio to improve its photocatalytic activity.

4. Conclusions

Optimal values for parameters of the SP technique were reached in order to have ZnO films with $1 \times 0.7 \, cm^2$ dimensions and only formed by nanoleafs or micro-cauliflowers. Varying the SP parameters it is possible to synthesize micron and submicron particles with cauliflower shape whose dimensions depend on Ms.

XRD results indicate an invariant hexagonal crystalline structure for ZnO cauliflower or ZnO nanoleaf when Ms or Tr vary. The film has a preferred and moderated growth in (100) or (002) directions when Ms or Tr increase, respectively. Grain size as a function of Ms rises until reaching 35 nm for Ms = 0.032 mol while grain size as a function of Tr remains constant in 35 nm for $350 \, °C < Tr < 450 \, °C$.

The optical measurements show there were not considerable differences between the optical properties of nanoleafs and cauliflower particles. Deconvolution of PL emission spectra made it possible to elucidate the existence of oxygen vacancies, interstitial oxygen, zinc vacancies and interstitial zinc, structural defects in nanoleafs and micro-cauliflowers.

V_O, O_i and V_{Zn} defects play an important role into PL and CL visible emissions of ZnO because electronic transitions associated to these defects origin almost the 100 % of these emissions.

Nanostructured ZnO cauliflowers with great potential application in photocatalysis were synthesized by a simple, scalable and low cost method.

References

[1] M. Mehedi Hassan, Wasi Khan, Ameer Azam, A.H. Naqvi, J. Lumin. 145 (2014) 160–166.
[2] G.Z. Shen, C.J. Lee, Cryst. Growth Des. 5 (2005) 1085–1089.
[3] Y. Zheng, C. Chen, Y. Zhan, X. Lin, Q. Zheng, K. Wei, J. Zhu, Y. Zhu, Inorg. Chem. 46 (2007) 6675–6682.
[4] C.H. Liu, J.A. Zapien, Y. Yao, X.M. Meng, C.S. Lee, S.S. Fan, Y. Lifshitz, S.T. Lee, Adv. Mater 15 (2003) 838–841.
[5] Zhicheng Yang, Qing Zhao, Yongxi Ou, Wei Wang, Heng Li, Dapeng Yu, Appl. Phys. Lett. 101 (2012) 173107.
[6] J.G. Reynolds, C.L. Reynolds Jr., A. Mohanta, J.F. Muth, J.E. Rowe, H.O. Everitt, D.E. Aspnes, Appl. Phys. Lett. 102 (2013) 152114.
[7] Ü. Özgür, Ya. I. Alivov, C. Liu, et al., J. Appl. Phys. 98 (2005) 041301.
[8] Zhang Lin-Li, Guo Chang-Xin, Chen Jian-Gang, Hu Jun-Tao, Chin. Phys. 14 (2005) 586.
[9] Z.R. Dai, Z.W. Pan, Z.L. Wang, Adv. Funct. Mater 13 (2003) 9–24.
[10] X.Y. Kong, Y. Ding, R. Yang, Z.L. Wang, Science 303 (2004) 1348–1351.
[11] A. Mitra, R.K. Thareja, V. Ganesan, A. Gupta, P.K. Sahoo, V.N. Kulkami, Appl. Surf. Sci. 174 (2001) 232–239.
[12] A. Pfahnl, J. Electrochem. Soc. 109 (1962) 502–507.
[13] Li Zhen-hua, Li Ying-yi, Zhong Dan, Xu Xin, Li Yong-xiu, J. Lumin. 128 (2008) 1758–1762.
[14] Fenglin Xian, Xiaoxiong Wang, Linhua Xu, Xiangyin Li, Wangfeng Bai, J. Lumin. 144 (2013) 154–157.
[15] Qing Lan Ma, Rui Xiong, Bao-gai Zhai, Yuan Ming Huang, Appl. Surf. Sci. 324 (2015) 842–848.
[16] Y.Q. Fu, J.K. Luo, X.Y. Du, A.J. Flewitt, Y. Li, G.H. Markx, A.J. Walton, W.I. Milne, Sens. Actuators B 143 (2010) 606–619.
[17] Zhong Lin Wang, Adv. Mater. 19 (2007) 889–892.
[18] M. Ashokkumar, S. Muthukumaran, J. Lumin. 162 (2015) 97–103.
[19] F. Golmar, M. Villafuerte, A. Mudarra Navarro, C.E. Rodriguez Torres, J. Barzola-Quiquia, P. Esquinazi, S.P. Heluani, J. Mater Sci. 45 (2010) 6174–6178.
[20] M. Guo, P. Diao, S. Cai, Thin Solid Films 515 (2007) 7162–7166.
[21] X. Feng, L. Feng, M. Jin, J. Zhai, L. Jiang, D. Zhu, J. Am. Chem. Soc. (2004) 63, 126-1.
[22] Cosmetics formulation comprising ZnO nanoparticles USPTO Patent Application 20050255057, Andre, Valerie , Brotzman Jr., Richard W. (Naperville, IL, US) 〈http://www.freepatentsonline.com/y2005/0255057.html〉 2005 (accessed 20.09.2015).
[23] Z.L. Wang, Mater. Today 7 (2004) 26–33.
[24] Olivera Milogevic, Vladimir Gagic, Joze Vodnik, Aleksandra Mitrovic, Ljiljana Karanovic, Biljana Stojanovic, Ljiljana Zivkovic, Thin Solid Films 296 (1997) 44–48.
[25] Sang Duck Lee, Sang-Hun Nam, Myoung-Hwa Kim, Jin-Hyo Boo, Phys. Procedia 32 (2012) 320–326.
[26] Nora S. Portillo-Vélez, Monserrat Bizarro, J. Nanomater. (2016) (2016) 1–11.
[27] S. Sakthivel, B. Neppolian, M.V. Shankar, B. Arabindoo, M. Palanichamy, V. Murugesan, Solar Energy Mater. Solar Cells 77 (2003) 65–82.
[28] B.D. Cullity, Elements of X-Ray diffraction, First Edition, Addison-Wesley Publishing company, Massashuetts, 1956.
[29] J.W. Zhao, LR. Qin, Z.D. Xiao, L.D. Zhang, Mater. Chem. Phys. 105 (2007) 194–198.
[30] A. Zendehnam, M. Mirzaee, S. Miri, Bull. Mater. Sci. Indian Acad. Sci. 37 (2014) 179–183.
[31] Gustav Kortüm, Reflectance Spectroscopy, First Edition, Springer-Verlag New York Inc., 1969, chap. 4.
[32] Y. Segawa, A. Ohtomo, M. Kawasaki, H. Koinuma, Z.K. Tang, P. Yu, G.K.L. Wong, Phys. Stat. Sol. (b) 202 (1997) 669–672.
[33] P. Yu, Z.K. Tang, G.K.L. Wong, M. Kawasaki, A. Ohtomo, H. Koinuma, Y. Segawa, Solid State Commun. 103 (1997) 459–463.
[34] Z.K. Tang, G.K.L. Wong, P. Yu, M. Kawasaki, A. Ohtomo, H. Koinuma, Y. Segawa, Appl. Phys. Lett. 72 (1998) 3270.
[35] Y. Fang, Q. Pang, X. Wen, J. Wang, S. Yang, Small 2 (2006) 612–615.
[36] M.K. Li, D.Z. Wang, S. Ding, Y.W. Ding, J. Liu, Z.B. Liu, Appl. Surf. Sci. 253 (2007) 4161–4165.
[37] M. Izaki, T. Shinagawa, H. Takahashi, J. Phys. D: Appl. Phys. 39 (2006) 1481–1484.
[38] Y. Segawa, H.D. Sun, T. Makino, M. Kawasaki, H. Koinuma, Phys. Stat. Sol. (a) 192 (2002) 14–20.
[39] H. Gao, F. Yan, J. Li, Y. Zeng, J. Wang, J. Phys. D: Appl. Phys. 40 (2007) 3654–3659.
[40] K.K. Kim, N. Koguchi, Y.W. Ok, T.Y. Seong, S.J. Park, Appl. Phys. Lett. 84 (2004) 3810.
[41] K. Vanheusden, W.L. Warren, C.H. Seager, D.R. Tallant, J.A. Voigt, B.E. Gnade, J. Appl. Phys. 79 (1996) 7983.
[42] A.B. Djurišic, et al., Adv. Funct. Mater. 14 (2004) 856–864.
[43] F.A.N. Hai-Bo, Y.A.N.G. Shao-Yan, Zhang Pan-Feng, W.E.I. Hong-Yuan, L.I. U. Xiang-Lin, J.I.A.O. Chun Mei, Z.H.U. Qin-Sheng, C.H.E.N. Yong-Hai, W.A.N. G. Zhan-Guo, Chin. Phys. Lett. 24 (2007) 2108.
[44] Gugu H. Mhlongo, David E. Motaung, Steven S. Nkosi, H.C. Swart, Gerald F. Malgas, Kenneth T. Hillie, Bonex W. Mwakikunga, Appl. Surf. Sci. 293 (2014) 62–70.
[45] P.S. Xu, Y.M. Sun, C.S. Shi, F.Q. Xu, H.B. Pan, Nucl. Instrum. Meth. Phys. Res. B 199 (2003) 286.
[46] H. Félix-Quintero, J. Angulo-Rocha, S.H. Murrieta, A.J. Hernández, G. E. Camarillo, J.M.C. Flores, C. Alejo-Armenta, M. García-Hipolito, F. Ramos-Brito, J. Lumin. 182 (2017) 107–113.
[47] Yuanhui Zheng, Chongqi Chen, Yingying Zhan, Xingyi Lin, Qi Zheng, Kemei Wei, Jiefang Zhu, Yingjie Zhu, Inorg. Chem. 46 (2007) 6675–6682.
[48] Bixia Lin, Zhuxi Fu, Yunbo Jia, Appl. Phys. Lett. 79 (2001) 943.
[49] S.A.M. Lima, F.A. Sigoli, M. Jafelicci Jr, M.R. Davolos, Int. J. Inorg. Mater. 3 (2001) 749–754.
[50] F.A.N. Hai-Bo, et al., Chin. Phys. Lett. 7 (2007) 2108–2111.
[51] Vladimir Nikitenko, Springer Netherlands 194, 2005, pp. 69–81.
[52] P.A. Rodnyi, I.V. Khodyuk, Opt. Spectrosc. 111 (2011) 776–785.
[53] Chih-Cheng Lin, Yuan-Yao Li, Mater. Chem. Phys. 113 (2009) 334–337.
[54] L. Ozawa, Cathodoluminescence: Theory and Applications Kodansha, Ltd., Tokyo, Japan and VCH Publishers, New York, USA, 1990, chap. 2.
[55] S. Myhajlenco, in: D.R. Vij (Ed.), Luminescence of Solids, Plenum Press, New York, 1998, chap. 4.
[56] Anna Mclaren, Teresa Valdes-Solis, Guoqiang Li, Shik Chi Tsang, J. Am. Chem. Soc. 9 (131) (2009) 12541.